Available online at www.sciencedirect.com

ScienceDirect

Procedia CIRP 107 (2022) 558–563

www.elsevier.com/locate/procedia

55th CIRP Conference on Manufacturing Systems

Implementation of a multi-material mechanism in a laser-based powder bed fusion (PBF-LB) machine

Thomas Bareth[a]*, Maximilian Binder[a,b], Philipp Kindermann[a], Veronika Stapff[a,c], Armin Rieser[a], Christian Seidel[a,c]

[a]*Fraunhofer IGCV (Institute for Casting, Composite and Processing Technology), Am Technologiezentrum 10, 86159 Augsburg, Germany*
[b]*Technical University of Munich, Institute for Machine Tools and Industrial Management, Boltzmannstr. 15, 85748 Garching, Germany*
[c]*Munich University of Applied Sciences, Department of Applied Sciences and Mechatronics, Lothstr. 34, 80335 Munich, Germany*

* Corresponding author. Tel.: +49821 90678314; fax: +49821 906780. *E-mail address:* thomas.bareth@igcv.fraunhofer.de

Abstract

Multi-material additive manufacturing by laser-based powder bed fusion (PBF-LB) combines the advantages of additive manufacturing (AM), such as the ability to build complex structures, with the capability to create an arbitrary material distribution in one manufacturing process. This paper presents the implementation of a multi-material mechanism in a mono-material PBF-LB system. Therefore, the multi-material process and the new powder deposition mechanism are introduced. Special attention is paid to the required process steps of powder recoating and powder removal. To gain further insight into the multi-material process, dependencies between the powder removal and the manufacturing quality are described. Furthermore, the required equipment and the current challenges of multi-material additive manufacturing are highlighted. In addition, results of the material combination consisting of the tool steel 1.2709 and the copper alloy CW106C are shown and discussed.

Keywords: metal additive manufacturing; laser powder bed fusion; multi-material; laser beam melting; PBF-LB/MM

1. Introduction

Additive manufacturing (AM) enables the layer-by-layer fabrication of complex, three-dimensional parts. As a result, there are significant advantages, such as the increased potential for functional integration [1, 2]. This already worthwhile achievement is taken to a new level by multi-material additive manufacturing. Multi-material additive manufacturing enables an arbitrary material distribution in components [3–5]. Thus, it is possible to combine material properties to maximize performance and functionality in a way that leads to enhanced advantages and performance for the application. This allows an unprecedented new scope for the design of parts.

For example, components can be manufactured in which the thermal conductivity differs within specific areas of the component. As a result, produced heat, for instance, in an injection nozzle [6], can be dissipated rapidly along areas of high thermal conductivity. This would be especially useful in components that do not have enough space for cooling channels. By adequately combining a material with high thermal conductivity with a harder material as the structural material, the mechanical properties of the entire component can be ensured. Besides other promising material combinations, the combination of electrically conductive materials with electrically insulating materials also has great potential [7].

10.1016/j.procir.2022.05.025

This paper describes the process of enabling a mono-material powder bed fusion (PBF) machine using a laser beam (-LB), for multi-material fabrication (PBF-LB/MM).

2. Method and Setup

2.1. Process steps of multi-material PBF-LB

There are various approaches for applying powders in a multi-material process [7–10]. One approach, which is very similar to the conventional PBF-LB recoating method, combines a full-surface powder application with powder removal by suction [8]. Here, two different powder materials are applied by pairing the conventional powder supplier with an additional powder conveying system for a second material. The individual process steps of this multi-material PBF-LB process are shown schematically in Figure 1.

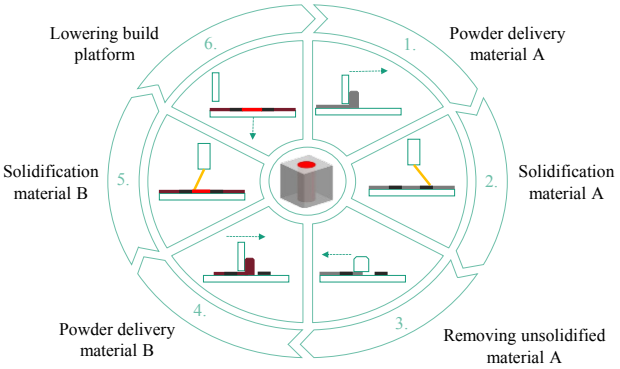

Figure 1. Process steps of multi-material PBF-LB, modified from [11].

At first, the recoater pushes material A from the supplier to the build plate, same as in the mono-material recoating process (step 1). Then, the applied powder of material A is selectively melted and solidified through laser radiation (step 2). In the third step, a suction unit removes the unsolidified powder of material A. The suction unit has the width of the build plate diameter, is mounted on the recoating slider and moves from right to left above the build plate, cf. Figure 2.

After the suction process, the powder of material B is delivered (step 4) and can be solidified (step 5).

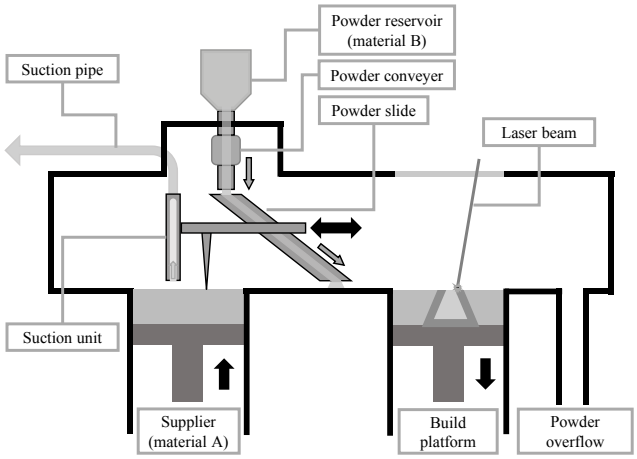

Figure 2. Schematic illustration of the developed multi-material system which was installed in the AconityONE PBF-LB machine.

2.2. Setup of the multi-material system

In the context of this investigation, a conventional mono-material PBF-LB machine was upgraded with a multi-material module (cf. Figure 3) for multi-material additive manufacturing. Hereby, an AconityONE machine was utilized due to its open interfaces for soft- and hardware modifications. The developed module contains adaptations of the recoater, which are located inside the process chamber, as well as several components, which are installed outside the process chamber. The developed multi-material module is mobile and can be installed and removed.

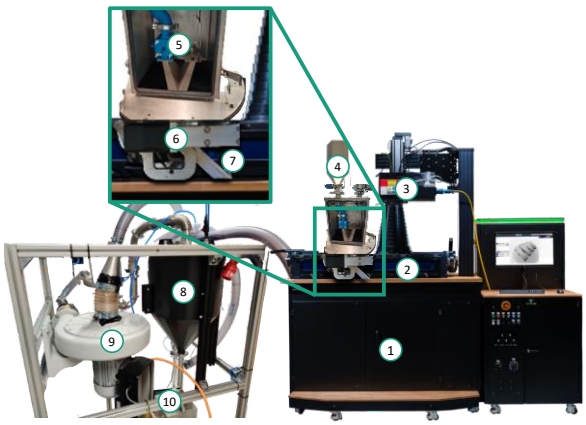

Figure 3. AconityONE together with the multi-material module.
1: AconityONE; 2: Process chamber; 3: Scan head; 4: Powder reservoir (material B); 5: Powder conveyor; 6: Recoater and suction unit; 7: Powder slide; 8: Cyclone separator; 9: Vacuum pump; 10: Electronic control unit.

Figure 3 shows the required components for the powder application of the second material (material B), with the powder reservoir (number 4), the powder conveyer (number 5) and the powder slide (number 7). In this case, the powder conveyor consists of a brush rotor, driven by an electric motor, which delivers a controllable amount of powder.

In addition, an energy chain-guided pipe connection leads from the suction unit (number 6) inside the process chamber to the outside-located further components. The powder gas mixture exiting the process chamber is directed through a pipe connection first to a cyclone separator (number 8) and then to the vacuum pump (number 9). The cyclone separator has the task of separating the degraded powder from the inert gas so that no powder particles enter the vacuum pump or re-enter the process chamber. The vacuum pump is required to generate the suction to remove the unsolidified powder of material A. For this purpose, the radial ventilator HRD 2T FUK#-95/3.0 (Elektror, Germany) is installed. A variable speed drive (1-100 %) is integrated within the ventilator at a maximum speed of 5,600 rpm (maximal volumetric flow rate V = 15.1 m³/min). Electrically switched hydraulic valves change between a bypass and the suction circuit.

The multi-material module can exchange signals with the AconityONE via the digital inputs and outputs using a built-in PLC (programmable logic controller) (Figure 3, number 10). It can thus be controlled directly from the AconityONE, which is necessary to realize the additive manufacturing process cycle, cf. Figure 1.

3. Experimental procedure and validation

In this study, similar to Anstaett et al. [12], the tool steel 1.2709 (X3NiCoMoTi18-9-5) is selected as material A and the copper alloy 2.1293 (also known as CuCr1Zr or CW106C) as material B for the multi-material additive manufacturing. Due to the high thermal conductivity of the copper alloy (310 W/mK at 20 °C [13]) and the high mechanical strength and hardness of the tool steel (yield strength = 1980 ± 7 MPa [14]; VHN_{300} (Vickers Hardness Number) = 599 [14]), these two materials complement each other through their contrasting properties. In addition, both materials can be separated effectively by magnetic sorting [15], which is an important aspect of powder recycling. In the investigations on recyclability of the mixed powders by Horn et al. [15], manual separation resulted in purities above 99 wt.% for the non-ferromagnetic component (CW106C), while the ferromagnetic powder material (1.2709) remained below 80 wt.% purity.

3.1. Powder removal analysis

Besides a homogeneous and full surface powder application, precise removal of the top powder layer (cf. step 3 in Figure 1) is fundamental to avoid undesired powder mixtures during multi-material powder application. For this reason, a method for verifying the powder application and the suction mechanism was developed.

First, the suction unit on the slider carriage is to be adjusted to a defined distance above the build plate by using feeler gauges (accuracy of +/- 0.05 mm). Two different suction distances (h = 1 mm and h = 2 mm) were defined. The width of the suction slot in the suction unit also has a high impact on the powder removal results. For the tests, the width of the suction slot was kept constant and is defined by the suction unit geometry.

Subsequently, five layers of tool steel (1.2709) powder were recoated to achieve a dense and homogenous powder surface on the build plate. Next, one layer of the copper alloy (CW106C) was recoated. The single layer thickness of the two materials was set at 30 µm, so that five layers of tool steel (1.2709) powder have a total height of 150 µm. An image of the powder bed on the build plate surface was taken from the top view of this set-up with a camera (Sony ILCE 6000 with SELP1650 lens) to record the recoating result. After this, the suction process started. At a constant travel speed (v = 35 mm/s), the slider carriage with the suction unit moved across the build plate from right to left. Both materials have a comparable density (1.2709: 8.1 g/cm³, CW106C: 8.9 g/cm³ [13]) and are assumed to behave similarly during the suction process.

The left part in Figure 4 shows the top view of the build plate surface with five recoated layers of tool steel (1.2709, in steel color) and one recoated CW106C layer (in copper color) on top. The right image in Figure 4 shows a top view of the same build plate after the completed suction process. In this case, suction at 50 % (2,800 rpm) of the maximum ventilator speed (5,600 rpm) was performed with a suction distance of h = 2 mm.

It is essential to reproduce the photographic results under consistent conditions to interpret the suction result at different ventilator speeds and suction distances. Therefore, the camera was fixed to a mounting. Furthermore, with an additional light source, efforts were made to ensure that the perspective of the image and the lighting conditions remained constant within the test series.

After suction, an area with the remaining CW106C powder can be seen in the lower part of the build plate. Stronger suction has removed more powder in the upper right area, and the build plate is visible here. This means that both the copper alloy (CW106C) layer and the five underlying layers of tool steel (1.2709) have been removed in this location.

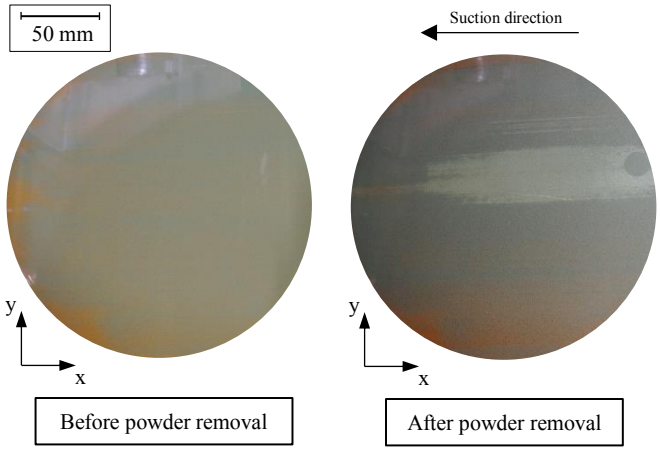

Figure 4. Top view of build plate (suction distance: h = 2 mm; ventilator speed: n = 2,800 rpm, suction travel speed: v = 35 mm/s).

An automated image processing method was developed to perform an objective analysis of the different images of the individual suction settings. Using a threshold evaluation in the software ImageJ, the area ratio of CW106C, 1.2709 and the visible build plate were determined. Figure 5 shows an example of a calculated threshold evaluation of the build plate surface after suction with the suction result from Figure 4 (right image). The areas marked in red correspond to the surface proportions of the respective material or the build plate itself.

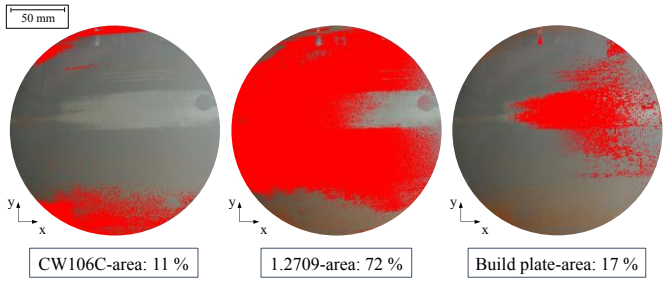

Figure 5. Area percentages calculated by threshold evaluation after suction on build plate surface (top view from Figure 4; suction distance: h = 2 mm; ventilator speed: n = 2,800 rpm, suction travel speed: v = 35 mm/s).

Figure 6 shows the result of a test series at a suction distance of h = 2 mm. Here, the distribution of the proportions on the build plate surface of CW106C, 1.2709 and the build plate at different ventilator speeds can be seen. With ideal suction parameters for the final multi-material process, only the 1.2709 powder should be visible from the top view on the build plate surface after this suction test. Because in this case, it can be assumed that at least one powder layer has been completely removed and also that in total, not more than six layers have been suctioned because the build plate is not yet visible.

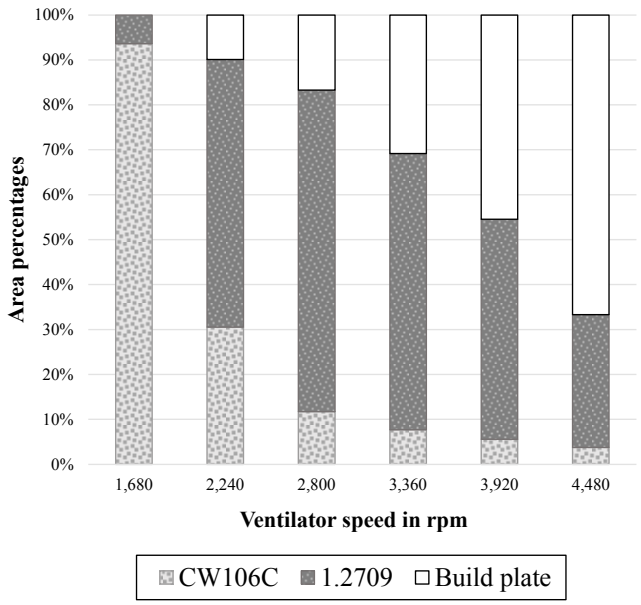

Figure 6. Results of the powder removal analysis with suction distance h = 2 mm (suction travel speed: v = 35 mm/s).

As a result of the test series in Figure 6, it can be observed that almost no powder is removed at a ventilator speed of 1,680 rpm. More than 90 % of the surface is still covered with CW106C powder. At the highest ventilator speed (4,480 rpm), most of the powder is removed from the build plate, and therefore the build plate itself can be seen in the predominant area of the build plate surface. However, when looking at the results of the test series (Figure 6), it is noticeable that in some surface areas copper alloy powder is still visible, while in other areas all six layers of powder have been removed.

3.2. Fabrication of multi-material test specimens

After the powder removal analysis, the results were taken to determine the functionality of the developed multi-material mechanism on the AconityONE. The following suction parameters were used for the fabrication of multi-material test specimens: Suction distance h = 2 mm, ventilator speed n = 2,500 rpm and travel speed v = 35 mm/s. Six cubes with the dimensions of 10x10x10 mm³ were built up as test specimens in a regular arrangement on the build plate (cf. Figure 7).

The test specimens consist of an outer shell and an inner core. The outer shell was built with tool steel (1.2709) and the inner core with the copper alloy (CW106C). As in the investigations of Anstaett [4], a discrete transition was chosen as the transition strategy between the outer shell and the inner core. To obtain a form-fit between the outer shell and the inner core, despite the different shrinkage properties of the two materials, a transition region was introduced, as done in the work of Anstaett [4]. The size of the transition zone was defined to be d = 0.4 mm.

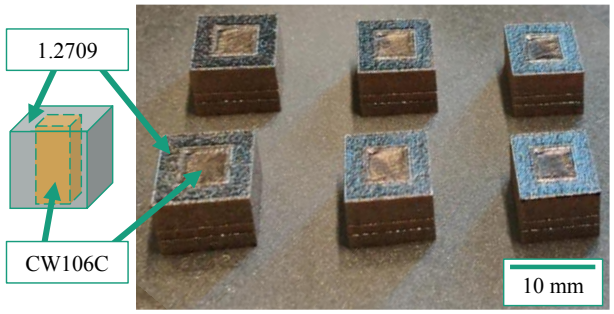

Figure 7. Multi-material test specimens (1.2709 area in grey color; CW106C area in copper color).

While manufacturing the test specimens, the tool steel (1.2709) was exposed first by the laser, followed by the copper alloy (CW106C) and the material transition zone. The used process parameters during this study are listed in Table 1.

Table 1. Applied process parameters.

Process parameters	Laser power in W	Laser speed in mm/s	Layer thickness in mm	Hatch distance in mm
1.2709	200	600	0.03	0.105
CW106C	400	400	0.03	0.125
Material transition zone (overlap)	400	400	0.03	0.125

3.3. Micrograph of the material transition zone

Following the fabrication of the test specimens, micrographs were prepared to investigate the material transition zone metallographically. An example of a generated micrograph of the transition zone is shown in Figure 8.

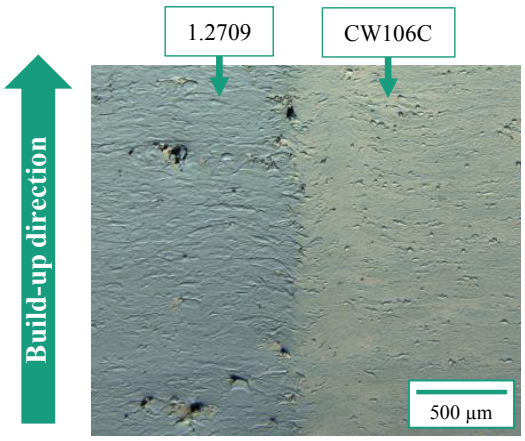

Figure 8. Micrograph of the test specimen, material transition zone between 1.2709 and CW106C.

Overall, a form fit in the material transition zone can be recognized. In addition, the mono-material areas appear dense. However, a higher level of porosity is visible in the 1.2709 area, where cross-contamination by CW106C powder is present. This can be observed by the CW106C contents surrounding the respective pores.

4. Discussion

The results of the suction tests (Figures 5 and 6) indicate that the suction is not perfectly homogeneous yet. Nonetheless, the developed module and method of proceeding for the powder removal analysis has been shown to be effective.

The non-ideal-homogeneously removal of the powder can be explained by the geometry of the suction unit. The suction unit was 3D-printed using FFF (Fused Filament Fabrication) technology with ABS (Acrylnitril-Butadien-Styrol-Copolymere) filament. Distortion has occurred due to the large part dimensions, which caused a convexity of the unit leading to an inconsistent distance between the suction unit and the build plate (the maximum height difference was 1.3 mm.). These results underline the need to re-design and re-fabricate a plane suction unit to achieve an even more homogeneous powder removal.

The functionality of the multi-material upgrade for the AconityONE was validated by the fabrication of multi-material test specimens (Section 3.2). The porosity (Figure 8) can be explained by optimizable powder removal. Due to an inhomogeneous suction process, cross-contamination appears. Particles of material A remain on the build plate surface, and then potentially get solidified by the laser in the area intended for material B. However, since materials A and B have different melting temperatures and require other laser parameters, cross-contamination can result in unmelted powder due to too low energy input in contaminated regions. In Figure 8, this can be seen by the increased porosity in the 1.2709 zone, where CW106C particles are located in the near surrounding of each pore.

5. Summary and Outlook

This work presents a method and a module to upgrade conventional mono-material PBF-LB machines to allow multi-material processing. An AconityONE machine was used as a demonstrator. Besides describing the equipment used for this purpose, this study gives an insight into powder removal analysis and metallographic investigation of the transition zone between the two metal alloys used (1.2709 and CW106C). At the same time, core challenges are described, such as achieving a homogeneous suction or reducing cross-contamination. Finally, it was validated that the multi-material module presented in this research enables multi-material fabrication on an AconityONE.

In further studies, cross-contamination in the transition zone between different materials is to be minimized. To achieve this, the multi-material module should be further optimized in order to achieve an even higher process quality with regard to homogeneous powder removal by utilizing the suction module. It is assumed that, compared to the currently used polymer material (ABS), a more temperature-resistant material for the suction module, such as PEEK or metal, is needed. Thereby, a geometrical accuracy for the component itself and for the distance to the build plate should be ensured.

Lastly, the shown multi-material mechanism can be modified to qualify for the processing of more than two materials once the above-mentioned prerequisites are given. Building on the work of Singer et al. [16], further research will focus on multi-material additive manufacturing with three or even four different materials to allow for e.g. the processing of a structural material, a conductor material and an insulator by utilizing large-format build plates of 200 mm in diameter.

Acknowledgments

The authors express their sincere thanks to the State of Bavaria and its Bavarian Ministry of Economic Affairs, Regional Development and Energy StMWi for funding the "MULTIMATERIAL-Zentrum Augsburg" (engl. "Multi-material Center Augsburg"). Furthermore, the authors would like to thank Mr. Kurt Hartmann for his support in executing the practical experiments.

References

[1] Gebhardt, A. 2016. Additive Fertigungsverfahren. Additive Manufacturing und 3D-Drucken fuer Prototyping - Tooling - Produktion. Hanser; Ciando, Muenchen.
[2] Wohlers, T., Campbell, R. I., Diegel, O., Kowen, J., and Mostow, N. 2021. Wohlers report 2021. 3D printing and additive manufacturing: global state of the industry. Wohlers Associates, Fort Collins, Colorado.
[3] Anstaett, C., Seidel, C., and Reinhart, G. 2018. Herstellung von 3-D-Multimaterialbauteilen aus Kupfer-Chrom-Zirkonium und Werkzeugstahl 1.2709.
[4] Anstaett, C. 2020. Multimaterialverarbeitung mittels Laserstrahlschmelzen am Beispiel von metallischen Verbindungen mit der Kupferlegierung CW106C. Universitaetsbibliothek der TU Muenchen, Muenchen.
[5] Anstaett, C. 2017. Fabrication of 3D-Multi-Material Parts by Laser Beam Based Powder Bed Fusion.
[6] Schneck, M., Horn, M., Schindler, M., and Seidel, C. 2021. Capability of Multi-material Laser-based Powder Bed Fusion – Development and Analysis of a Prototype Large Bore Engine Component. MDPI Metals. Manuscript under review.
[7] Koopmann, J. Multimaterialdruck von integrierten elektrischen Strukturen mittels selektivem Laserschmelzen. Dissertation, Kassel University Press GmbH.
[8] Anstaett, C. and Seidel, C. 2016. Multi-Material Processing: Next step in laser-based powder bed fusion. Laser Technik Journal 13, 28–31.
[9] Rafiee, M., Farahani, R. D., and Therriault, D. 2020. Multi-Material 3D and 4D Printing: A Survey. Advanced science. 7, 12, 1902307.
[10] Neirinck, B., Li, X., and Hick, M. 2021. Powder Deposition Systems Used in Powder Bed-Based Multimetal Additive Manufacturing. Acc. Mater. Res. 2, 6, 387–393.
[11] Anstaett, C., Seidel, C., and Reinhart, G. 2018. Multi-Material Fabrication of Copper-Chrome-Zirconia and Tool Steel 1.2709 by Powder Bed Based Laser Beam Melting.
[12] Anstaett, C. 2017. Laser-based Powder Bed Fusion Of 3D-Multi-Material-Parts Of Copper-Chrome-Zirconia And Tool Steel.
[13] Schmelzmetall. 2021. Material Product Data Sheet: Hovadur CCZ (CW106C).https://www.schmelzmetall.com/fileadmin/downloads/pulver 3d/SMZMT211110-1_Datenblatt_HOVADUR-CCZ-additiv-gefertigt.pdf.
[14] Oerlikon metco. 2021. Material Product Data Sheet: MetcoAdd C300-A (1.2709).https://www.oerlikon.com/ecoma/files/DSM-0319.0_AM_MaragingSteel_C300.pdf?download=true.

[15] Horn, M., Prudzilko, P., Anstaett, C., Lutter-Guenther, M., and Reinhart, G. 2018. Powder Separation Strategies for Recycling in Multi-Material Additive Manufacturing.

[16] Singer, C., Schmitt, M., Schlick, G., and Schilp, J. 2021. Multi-material additive manufacturing of thermocouples by laser-based powder bed fusion. (accepted)